

Global Model For High-Power HBTs Suitable for CAD and Device Optimization

F. DHONDT¹, J. BARRETTE² and P.A. ROLLAND¹

¹Institut d'Electronique et de Microélectronique du Nord, 59652 Villeneuve d'Ascq, France
Tel : 33 (0) 3 20 19 79 20 Fax : 33 (0) 3 20 19 78 96 Email : francois.dhondt@iemn.univ-lille1.fr

²Avionics Directorate, AFRL, Wright-Patterson AFB, Ohio 45433, U.S.A.

ABSTRACT

In this paper the authors present a novel global simulation of multifinger HBTs. It is based on the reunion of several models in a commercial CAD software. Each electrical, electromagnetic and thermal model is also used to optimize the performance of devices having complex topologies. We show the typical result of large signal simulation performed with a microwave simulation tool. This model accurately predicts coupled thermal and electrical effects in multifinger power devices.

INTRODUCTION

Due to the technological maturity now achieved by the high power HBTs manufacturers, these devices are soon to be widely used in complex systems. Circuit and device design requires accurate, physics-based models which take into account not only electrical but thermal effects. A number of recent works (1,2,3,4) have led to charge-control models based on the Gummel-Poon bipolar model. One of the most complete models has been proposed by the University of San Diego (UCSD) in collaboration with the HBT Model Working Group (5); this group brings together several industrial partners and the U.S. Advanced Research Projects Agency (ARPA). In its complete version this model has more than ninety parameters and is to become an industrial standard for commercial simulation tools. The determination of all these parameters relies on the extensive characterization of numerous devices in various operation modes. With this approach it is very difficult to predict the electrical behavior of novel HBT structures.

Our predictive global model for high-power HBTs is built on a self-consistent correlation of results from physical, electromagnetic and thermal simulations. These individual models allow us to optimize proposed device topologies both electrically and thermally. In addition, we have coupled these models into a commercial CAD software (HP-MDS) to achieve realistic electrothermal simulations of InGaP/GaAs HBTs. Using this model we can predict the current collapse phenomenon (6), and we can accurately predict the large-signal performance of power HBT unit cells.

ELECTRICAL ANALYSIS / PHYSICAL SIMULATIONS

The electrical simulations are based on a non-stationary hydrodynamic model that solves the semiconductor and electrical equations in 1D or 2D with a finite-difference method. We use the alternative direction implicit (ADI) method that ensure a strong convergence in the resolution of these equations. The transport parameters are derived from Monte-Carlo simulations and are temperature dependent. Figure 1 depicts the evolution of the electrical field in the structure under various injection conditions. One can note the moving of the field's maximum with the injection condition. The typical evolution of the base-collector junction capacitance is presented in figure 2. The total depletion of the collector is represented by the minimum of this capacitance. With this physical electrical model it is then possible to extract the large and small signal electrical equivalent circuits of the intrinsic device for various bias conditions and temperatures under a step or RF response.

ELECTRICAL ANALYSIS / ELECTROMAGNETIC SIMULATIONS

The extrinsic parasitic elements are computed using the 3D electromagnetic simulator HP-HFSS (7). This method is justified by the complex topology of multifinger, thermally-shunted HBTs. In a typical structure depicted in figure 3, several propagation modes are present; namely, microstrip in zones A and E, coplanar in

zones B and D, and hybrid in zone C. With this last mode, the electrical field is principally in the air (or dielectric), under the bridge. The device is modeled as three sections: the base and collector access regions and the active device section. We compute the scattering parameters of these sections for numerous frequencies. Some parasitic resistances, such as that of the base access, are evaluated using classic analytical laws.

Within HP-MDS, we use black-box representations for the access regions, whereas the coupling capacitances in the active region are computed using an S to Y parameter transformation. This method has been validated by on-wafer measurements performed on passive HBTs. The modeled parasitic capacitance values agree with measurements to within 20%. Based on this validation, we performed design studies of the impact of changes in HBT topology on parasitic coupling. Figure 4 shows the influence of the thickness of the dielectric between the base metal and the emitter pillar metal on base-emitter parasitic capacitance. Also shown for reference is the calculated geometric capacitance; the 27 fF difference between the two curves is likely due to radiative coupling at the edges of the metallizations. With this method it is possible to localize the origins of coupling parasitics and develop solutions to minimize them.

Finally, we used this method of parasitic extraction to study coupling effects for a variety of topologies. For example, figure 5 depicts an HBT design in which five circular emitter contacts of 4 μm diameter comprise the emitter finger. For an equivalent emitter area of 60 μm^2 the computed capacitances are:

$$C_{be} = 24 \text{ fF} \quad C_{bc} = 8.2 \text{ fF} \quad C_{ce} = 31 \text{ fF}$$

For this topology base-emitter capacitance is about half that of the HBT with rectangular emitter, while base-collector capacitance is slightly larger. It should be noted that this topology differs from the previous topology in that the design in figure 5 has no interlayer dielectric covering the emitter.

THERMAL ANALYSIS

In addition to extrinsic electrical parasitics, thermal characteristics of complex HBT structures can't be easily calculated. Temperature has a strong influence on electrical performance in HBTs but also on the thermal properties of the materials (e.g. GaAs). Electrothermal feedback within the active region of the device and poor GaAs thermal conductivity lead to a non-linear electrothermal system. Simple analytical calculations models are not accurate in predicting maximum junction temperature for arbitrary topologies, so we must employ a 3D numerical computation. Commercially-available thermal and electrothermal simulation tools (e.g. Aries[®], ANSYS[®]) are typically limited by their demand for substantial computer resources, being based on the finite-elements method. In many commercial packages, a uniform power dissipation is assumed, neglecting the electrothermal feedback present in HBTs. We have developed a custom software named HETMOS (HBT ElectroThermal MOdeling Software) that solves the heat flow equation in three dimensions coupled with current injection and current gain laws (8). It takes into account realistic boundary conditions: conduction through the substrate as well as convection and radiation by the top surface. It was developed under Windows 95 with a user friendly interface (figure 6). The model calculates the temperature and current distributions for an arbitrary bias point and an arbitrary HBT topology.

With this tool we have rigorously identified the thermal runaway effect in multifinger devices under constant base current operation. The simulated versus measured current collapse effect is depicted in figure 7. This effect is the combination of cumulative thermal effects and localized high current density that leads to a current gain fall-off. Essentially, hot spots form in the vicinity of the central fingers as electrothermal feedback and thermal coupling causes the central fingers to consume more and more of the base current, thus de-activating the lateral fingers.

We have also used the 3D electrothermal model to optimize the thermal design of InGaP/GaAs HBTs employing emitter ballast resistance and thermal shunt. Figure 8 shows the influence of the emitter finger spacing on device thermal resistance and maximum temperature, while figure 9 shows the stabilizing effect of emitter ballast resistance on the thermal runaway threshold.

DYNAMIC ELECTROTHERMAL MODEL

The results of electrical and thermal simulations are inserted into the CAD software HP-MDS using spline interpolation tables. We use the internal software convergence procedure to find the equilibrium solution between these models: the output data (I-V) computed by the temperature-dependent electrical model are inserted into the thermal model to find the new temperature. With an iterative method the final temperature and electrical parameters are rapidly found. This method can be used to perform DC simulations as well as prediction of large-signal performance. For a small-signal analysis there is no interaction between the electrical and thermal models, whereas in a large-signal simulation, where the output power contributes to the energy balance, this interaction is taken into account.

Figure 10 shows a typical large signal simulation. The optimum input and output impedances for a 4-finger device have been measured by Thomson's Central Research Laboratory and at IRCOM (Limoges – France). We can see the good agreement between the source impedance. The error between our model and the two other measurements for the load impedance is not significant. The non-linear behavior of our model is depicted in figure 11. We see the evolution of power added efficiency (P.A.E.) as a function of input power; also shown is the evolution of the base current that results from the self-bias phenomenon.

CONCLUSION

In this paper we have described our novel method for the global modeling of complex multifinger HBTs. This method can be used to optimize the topology of the device from a thermal or electrical point of view and to perform large-signal simulation as well.

ACKNOWLEDGEMENT

This work was supported by the French Ministry of Defense (DRET). The InGaP/GaAs HBTs were provided by Thomson-LCR.

REFERENCES

- (1) P. Grossman and J. Choma, *IEEE Trans. Microwave Theory Tech.*, 1992, **40**, p. 449.
- (2) K. Lu, P.A. Perry and T.J. Brazil, *IEEE Trans. Microwave Theory Tech.*, 1995, **43**, p. 1433.
- (3) Q.M. Zhang, H. Hu, J. Sitch, R.K. Surridge and J.M. Xu, *IEEE Trans. Microwave Theory Tech.*, 1996, **44**, p. 2001.
- (4) C.M. Snowden, *IEEE Trans. Microwave Theory Tech.*, 1997, **45**, p. 58.
- (5) L.H. Camnitz, S. Kofol, T. Low and S.R. Bahl, *Characterization Solutions*, HP EEsof Technical Publication Vol. 3, Issue 1, 1998, p. 1.
- (6) W. Liu, S. Nelson, D. Hill and Khatibzadeh, A., *IEEE Trans. Electron Devices*, 1993, **40**, p. 1917.
- (7) F. Dhondt, J. Barrette, N. Haese, P.A. Rolland and S.L. Delage, "Finite-Element Characterization of Parasitics in Multifinger, Thermally Shunted HBTs", *IEEE MGWL*, Vol. 8, n°4, 1998.
- (8) F. Dhondt, J. Barrette and P. A. Rolland, "3D finite difference electrothermal model for multifinger HBTs with thermal shunt and emitter ballast resistance", *IEE Solid-State Electronics*, to appear 1998.

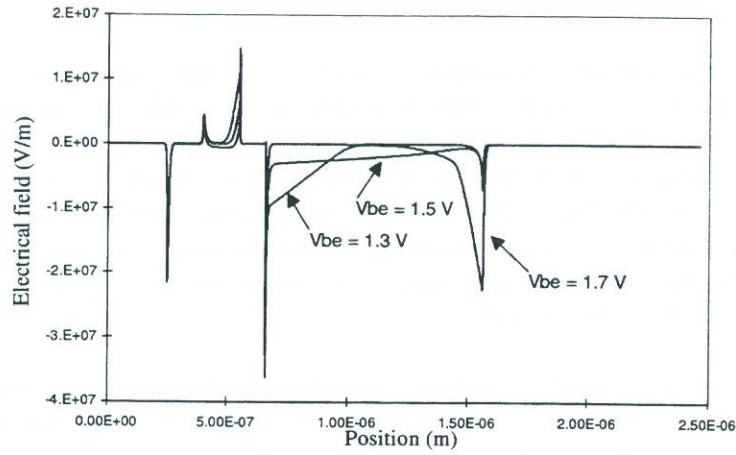


Fig. 1 - Simulated electric field versus position for InGaP/GaAs HBT, calculated from 1D hydrodynamic electrical model, as a function of bias.

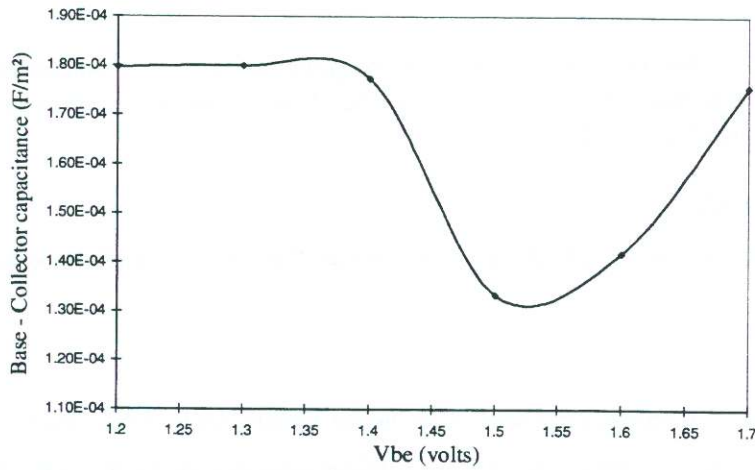


Fig. 2 - Calculation of base-collector junction capacitance from 1D hydrodynamic model results.

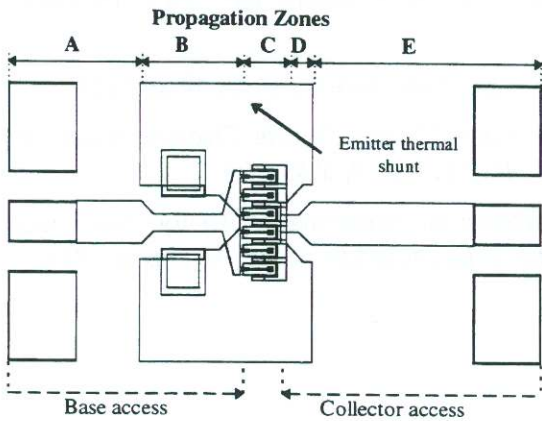


Fig. 3 - Schematic of thermally-shunted HBT.

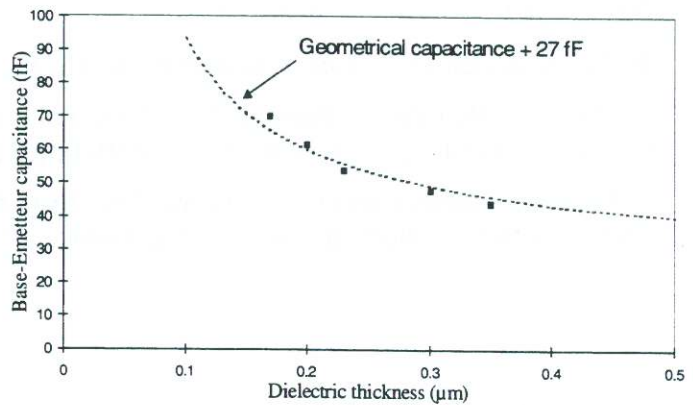


Fig. 4 - Modeled parasitic base-emitter capacitance as a function of interlayer dielectric thickness.

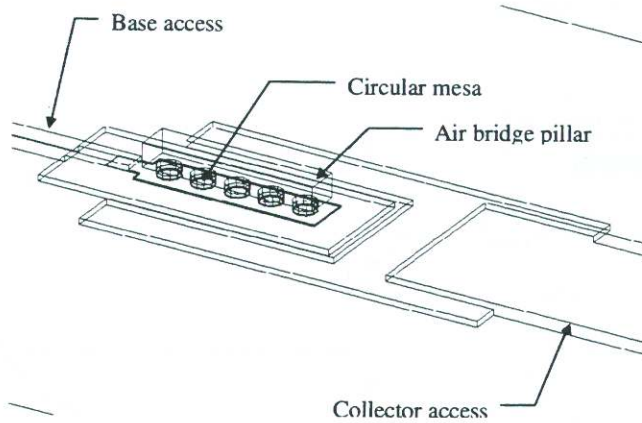


Fig. 5 - Simulated single-finger HBT with thermal shunt and circular emitter contacts.

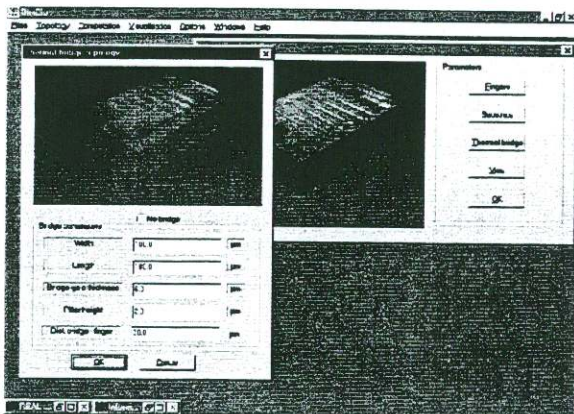


Fig. 6 - 3D Electrothermal model interface.

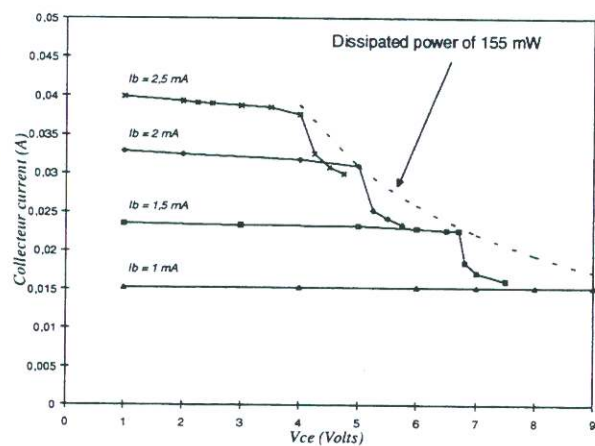


Fig. 7 - Simulated versus modeled collector current collapse in un-ballasted HBT.

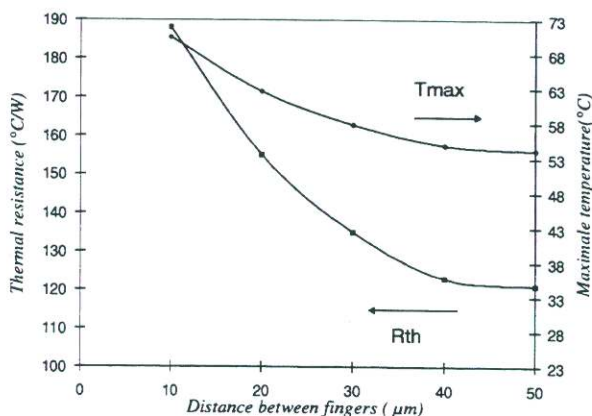


Fig. 8 - Simulated thermal resistance and maximum temperature as a function of finger spacing for a 4-finger HBT with thermal shunt.

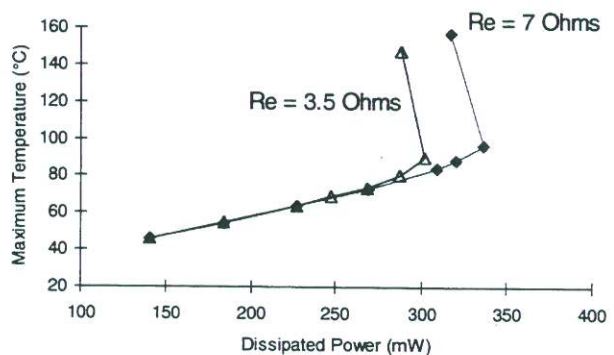


Fig. 9 - Simulated maximum temperature as a function of dissipated power for two values of emitter ballast resistance.

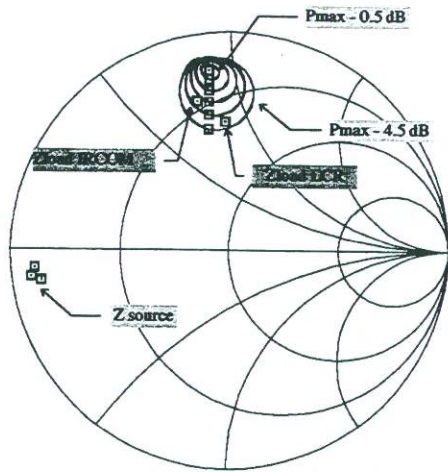


Fig. 10 - Measured versus simulated load-pull results for InGaP/GaAs HBT.

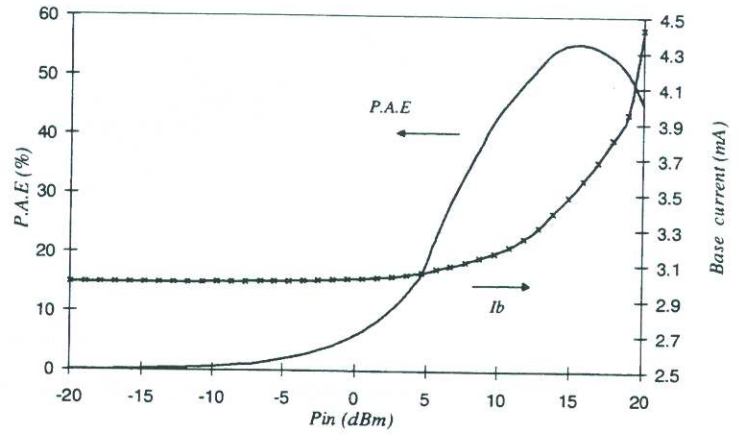


Fig. 11 - Simulated P.A.E. and base current as a function of input power for InGaP/GaAs HBT.